NMR Structure of the [2Fe-2S] Ferredoxin Domain from Soluble Methane Monooxygenase Reductase and Interaction with Its Hydroxylase[†,‡]

Jens Müller,[§,||] Alexey A. Lugovskoy,[||,⊥] Gerhard Wagner,*[,||] and Stephen J. Lippard*[,§]

Department of Chemistry, Massachusetts Institute of Technology, Cambridge, Massachusetts 02139-4307, Department of Biological Chemistry and Molecular Pharmacology, Harvard Medical School, Boston, Massachusetts 02115-5730, and Committee on Higher Degrees in Biophysics, Harvard University, Cambridge, Massachusetts 02138-3800

Received August 10, 2001; Revised Manuscript Received October 14, 2001

ABSTRACT: The soluble methane monooxygenase (sMMO) from *Methylococcus capsulatus* (Bath) is a multicomponent enzyme system required for the conversion of methane to methanol. It comprises a hydroxylase, a regulatory protein, and a reductase. The reductase contains two domains: an NADH-binding and FAD-containing flavin domain and a ferredoxin (Fd) domain carrying a [2Fe-2S] cofactor. Here, we report the solution structure of the reduced form of the 98-amino acid Fd domain (Blazyk, J. L., and Lippard, S. J. Unpublished results) determined by nuclear magnetic resonance (NMR) spectroscopy and restrained molecular dynamics calculations. The structure consists of six β strands arranged into two β sheets as well as three α helices. Two of these helices form a helix−proline−helix motif, unprecedented among [2Fe-2S] proteins. The [2Fe-2S] cluster is coordinated by the sulfur atoms of cysteine residues 42, 47, 50, and 82. The 10.9 kDa ferredoxin domain of the reductase protein transfers electrons to carboxylate-bridged diiron centers in the 251 kDa hydroxylase component of sMMO. The binding of the Fd domain with the hydroxylase was investigated by NMR spectroscopy. The hydroxylase binding surface on the ferredoxin protein has a polar center surrounded by patches of hydrophobic residues. This arrangement of amino acids differs from that by which previously studied [2Fe-2S] proteins interact with their electron-transfer partners. The critical residues on the Fd domain involved in this binding interaction map well onto the universally conserved residues of sMMO enzymes from different species. We propose that the [2Fe-2S] domains in these other sMMO systems have a fold very similar to the one found here for *M. capsulatus* (Bath) MMOR−Fd.

Nature has evolved a variety of enzymatic systems capable of oxidizing hydrocarbons using dioxygen as the oxidant. Included are cytochrome P450 monooxygenase (*1*), alkene monooxygenase (*2*), phenol hydroxylase (*3*), and different toluene monooxygenases (*4, 5*). Among the most interesting of these systems are the methane monooxygenases (MMOs)[1] because they have the ability to oxidize methane, the most stable of all of the hydrocarbons. This process is of considerable biological, chemical, and industrial importance (*6*−*10*). Both soluble and membrane-bound MMOs are expressed in methanotrophic bacteria that use methane as their sole source of carbon and energy.

Among the best-studied of hydrocarbon oxidizing enzymes is the soluble methane monooxygenase from *Methylococcus capsulatus* (Bath). It comprises three protein components: a carboxylate-bridged diiron-containing hydroxylase MMOH (251 kDa), a regulatory protein MMOB (15.9 kDa), and a reductase MMOR (38.7 kDa) (*11, 12*). Three-dimensional structures of MMOH (*13*−*17*) and MMOB (*18, 19*) from this and another organism have already been reported, whereas the MMOR protein has not yet been structurally characterized, despite its important role in the catalytic cycle (*11, 20*−*24*). MMOR contains two prosthetic groups, a [2Fe-2S] cluster and an FAD moiety, which facilitate electron transfer from NADH to MMOH. The [2Fe-2S] cluster is located in the N-terminal region of MMOR. Its spectroscopic properties, including results from Mössbauer, optical, and EPR measurements (*20, 22, 24, 25*), are similar to those exhibited by other plant-type ferredoxins. Both the FAD cofactor and NADH binding site are located in the C-terminal part of MMOR.

Several structures of [2Fe-2S] proteins have been determined, most of them by X-ray crystallography (see, for example, refs *26*−*28*). Only a few [2Fe-2S] protein structures solved by nuclear magnetic resonance (NMR) methods have appeared in the protein data bank (*29*), all of them in the oxidized $Fe^{III}Fe^{III}$ form of the metal cluster (*30*−*35*). These plant-type ferredoxins contain two iron and two inorganic

[†] This work was supported by the National Institute of General Medical Sciences Grants GM38608 to G.W. and GM32134 to S.J.L.

[‡] Structures have been deposited with the Brookhaven PDB database (PDB ID code 1JQ4). Chemical shifts have been deposited with the BioMagResBank (BMRB accession code 5148).

* To whom correspondence should be addressed. E-mail: (G.W.) gerhard_wagner@hms.harvard.edu, (S.J.L.) lippard@lippard.mit.edu.

[§] Massachusetts Institute of Technology.

[||] Harvard Medical School.

[⊥] Harvard University.

[1] Abbreviations: Fd, [2Fe-2S] ferredoxin; FNR, ferredoxin−$NADP^+$ reductase; MMOB, regulatory protein of methane monooxygenase; MMOH, methane monooxygenase hydroxylase; MMOR, methane monooxygenase reductase; MMOR−Fd, ferredoxin domain of MMOR; PDR, phthalate dioxygenase reductase; sMMO, soluble methane monooxygenase.

10.1021/bi015668k CCC: $22.00
Published on Web 12/05/2001

sulfur atoms. They function as one-electron carriers, usually between membrane-bound ferredoxin proteins in photosystem I and ferredoxin-dependent enzymes or ferredoxin−$NADP^+$ reductase (FNR) (*36*, *37*). The 38.7 kDa size of MMOR and the presence of a paramagnetic [2Fe-2S] domain render it a challenging structure to determine by NMR spectroscopy. In part to facilitate this task, the individual [2Fe-2S] and FAD domains have been cloned and expressed in *Escherichia coli*.[2] In the present paper, we report the NMR solution structure of the reduced $Fe^{II}Fe^{III}$ form of the ferredoxin domain of MMOR and an analysis of its interaction with MMOH. Ultimately, the knowledge of the reductase structure together with the three-dimensional structure of MMOH will enable us to discuss long-range electron transfer within and between these proteins.

MATERIALS AND METHODS

Expression of MMOR−Fd. To produce an expression system for the methane monooxygenase reductase ferredoxin domain (MMOR−Fd) that gives high yields in M9 minimal medium required for isotope labeling, the plasmid pRED−Fd[2] containing the gene coding for MMOR−Fd was transformed into competent *E. coli* BL21(DE3) cells. These cells were grown at 37 °C on an M9 minimal medium supplemented with 0.25 mM $Fe(NH_4)_2(SO_4)_2{\cdot}6H_2O$ and containing ampicillin (100 mg L^{-1}) with constant shaking. When the OD_{600} of the cultures reached about 0.6 (0.4 in the case of a D_2O-containing medium), expression was induced by adding IPTG to a final concentration of 1 mM, and another 0.1 mM $Fe(NH_4)_2(SO_4)_2{\cdot}6H_2O$ was added. Four hours after induction, the cells were harvested by centrifugation (7800*g*, 5 min) and immediately suspended in 50 mL of a lysis buffer (20 mM Tris (pH 7.2), 8 mM sodium thioglycolate, 50 mM NaCl, 5 mM $MgCl_2$, 12.5 mg Pefabloc, 2 mM PMSF, and 15 μL of DNase I). Cells were lysed by sonication on ice for 3 × 2 min using 40% output power with a Branson Sonifier 450. The soluble cell extract was separated from insoluble material by centrifugation (180000*g*, 30 min), decanted, and filtered through 0.2 μm membranes. It was dialyzed for 2 × 90 min periods against 20 mM Tris (pH 7.2), 8 mM sodium thioglycolate, and 50 mM NaCl to prevent a high salt concentration on the following anion-exchange column.

The protein solution was loaded onto a DEAE CL-6B Sepharose column equilibrated with 20 mM Tris (pH 7.2), 8 mM sodium thioglycolate, and 50 mM NaCl (buffer A). After the column had been washed with 50 mL of 85% buffer A, MMOR−Fd was eluted with an 800 mL linear gradient from 50 to 500 mM NaCl at a flow rate of 1.0 mL min^{-1}. Fractions of MMOR−Fd, eluting around 370 mM NaCl, were pooled on the basis of SDS−PAGE gel analysis but could also be identified because of their intense brownish color. After concentration through a 10 kDa cutoff membrane, the crude protein solution was applied to a Superdex 75 size-exclusion column equilibrated with 25 mM MOPS (pH 7.0), 1 mM DTT, and 200 mM NaCl and eluted at a flow rate of 0.5 mL min^{-1}. Fractions containing MMOR−Fd were identified by SDS−PAGE gel analysis. After buffer exchange into 50 mM sodium phosphate (pH 7.0) and 1 mM DTT, the protein was frozen in liquid nitrogen and stored at −80 °C.

For the ^{15}N-labeled protein, the M9 minimal medium was prepared using 1 g L^{-1} $^{15}NH_4Cl$ (Cambridge Isotope Labs, Andover, MA). Uniform ^{13}C labeling was achieved by the use of 2 g L^{-1} ^{13}C glucose (Cambridge Isotope Labs, Andover, MA) in the medium and biosynthetic fractional ^{13}C labeling with 10% ^{13}C glucose (*38*). Triple-labeled samples were obtained from an M9 minimal medium supplemented with $^{15}NH_4Cl$, ^{13}C glucose, and 70% D_2O (Cambridge Isotope Labs, Andover, MA). Typical preparations led to the isolation of 2 mg (^{15}N,^{13}C,^{2}H labeled) to 12 mg (^{15}N labeled) of MMOR−Fd per liter of the M9 minimal medium. The concentration of MMOR−Fd was determined by using an extinction coefficient of $\epsilon_{458} = 9550\ M^{-1}\ cm^{-1}$.[2]

For the selective labeling of leucine and valine residues, the plasmid pRED−Fd was transformed into competent *E. coli* DL39 cells (auxotroph for Asp, Ile, Leu, Phe, Tyr, and Val). The resulting DL39/pRED−Fd cells were grown in an M9 minimal medium supplemented with 0.1 mmol L^{-1} $Fe(NH_4)_2(SO_4)_2{\cdot}6H_2O$ and 100 mg L^{-1} of each of the six amino acids. Either ^{15}N labeled leucine or valine was used. Reverse selective labeling of arginine residues was achieved by growing BL21(DE3)/pRED−Fd cells in an M9 minimal medium supplemented with 0.1 mmol L^{-1} $Fe(NH_4)_2(SO_4)_2{\cdot}6H_2O$, 1 g L^{-1} $^{15}NH_4Cl$ and 100 mg L^{-1} natural abundance arginine.

NMR Experiments. NMR experiments were performed on the reduced MMOR−Fd protein in 50 mM Na phosphate buffer (pH 7.0) with 1 mM DTT, 0.1% NaN_3, and 1 × Complete Mini EDTA free protease inhibitor cocktail (Roche Diagnostics, Germany). The addition of 1.5−3 equiv of $Na_2S_2O_4$ reduced the protein. The NMR tubes were filled under a nitrogen atmosphere and flame sealed.

Spectra were acquired at 750 MHz (Varian Unity Inova), 600 MHz (Bruker DRX), 500 MHz (Bruker DRX, Varian Unity or Varian Inova), or 400 MHz (Varian Unity Plus) at 25 °C. Backbone resonance assignments were obtained by using standard three-dimensional heteronuclear experiments (HNCA, HN(CO)CA, HN(CA)CB, HN(COCA)CB, and HNCO) and selective-labeling techniques (*39*). Side-chain assignments were obtained by using ^{15}N TOCSY−HSQC, HCCH−TOCSY, ^{15}N NOESY−HSQC, ^{13}C NOESY−HSQC, H(C−CO)NH−TOCSY, and (H)C(CO)NH−TOCSY experiments (*39*). Stereospecific assignments of six methyl groups were obtained with biosynthetic fractional ^{13}C labeling (*38*). Distance constraints were collected from ^{15}N NOESY−HSQC (100 ms mixing time), ^{13}C NOESY−HSQC (80 ms mixing time), and homonuclear proton NOESY experiments (100 ms mixing time). Spin−lattice relaxation times $T_{1\rho}$ of the ^{15}N amide nitrogen atoms were determined by fitting the respective peak intensities as measured by the peak height to a single-exponential fitting function (*40*, *41*). Spectra were processed with FELIX (Molecular Simulations Inc., San Diego, CA) and analyzed with XEASY (*42*) on Silicon Graphics workstations. Dihedral angle constraints for ϕ and ψ were obtained with TALOS (*43*).

Binding Studies. To characterize the interaction of MMOR−Fd with MMOH, NMR titration studies were performed in which ^{15}N,^{1}H HSQC spectra of ^{15}N-labeled MMOR−Fd were monitored upon addition of increasing amounts of unlabeled MMOH. The titration study was performed at MMOR−Fd

[2] Blazyk, J. L., and Lippard, S. J. Unpublished results.

concentrations of 0.2 mM and MMOH/MMOR−Fd ratios of 1:10, 1:6, and 1:2.4. NMR samples were equilibrated at 4 °C for 1 day before recording the spectra to ensure complete reduction of both MMOH and MMOR−Fd. To keep the samples reduced, 60 mM $Na_2S_2O_4$ and 3 mM NADH were used as reducing agents, giving rise to a final pH of 6.6. These experiments showed differential line broadening of the HSQC cross-peaks upon the addition of MMOH. As already noted in a related study (*18*), the equilibrium examined by NMR spectroscopy comprises a small protein in the free state and a large (262 kDa) complex in the bound state. On the basis of an empirical approximation for rotational correlation times (*44*), proton line widths in the range of 250 Hz can be estimated for a complex with this molecular weight, which would cause the signals of bound MMOR−Fd to be absent from the spectra. Because of chemical exchange with the bound state, the lines of the free form are expected to be broadened as well when excess MMOR−Fd is present. The amount of this line broadening depends inter alia on chemical shift differences between the free and bound forms. This effect can, therefore, be used to identify the binding surface, assuming that the resonances of the residues close to the contact surface experience the largest chemical shift changes (*45*). In the closely related system of MMOH and the regulatory protein MMOB, the validity of this approach was verified by using simulated line shapes (*18, 45*).

Structure Calculations. The volumes of the NOESY cross-peaks of assigned resonances were obtained by using the integration routines in the program XEASY (*42*). NOESY cross-peak intensities were converted into interatomic upper-distance limits by the program CALIBA (*46*). Initial structure calculations were performed on Silicon Graphics workstations with the program DYANA (version 1.5) using simulated annealing by molecular dynamics in torsion-angle space (*47*). A total of 1124 unambiguous NOEs (430 interresidue and 694 intraresidue) were used as distance constraints, supplemented with 18 distance constraints for the [2Fe-2S] cluster. The conformer with the lowest target function was then employed as a template for further calculations with the program X-PLOR (version 3.84) (*48*). At this stage of the calculations, a total of 88 residual dipolar coupling constraints were also implemented. For this purpose, amide proton-to-amide nitrogen couplings J_{NH} were measured in the modified Fast HSQC pulse sequence (*49*). In this sequence, the hard refocusing proton 180° pulse in the middle of the nitrogen chemical shift evolution period was substituted by two water-selective 90° pulses before and after this evolution period to maintain water at the $+z$ axis and to prevent radiation damping. The $J_{C\alpha CO}$ couplings were determined with a modified HNCO experiment (*50*). Alignment of the protein was achieved by adding 20 mg mL^{-1} of magnetic resonance cosolute phage Pf1 strain LPII-92 (Asla Ltd., Riga, Latvia) (*51*). Under these conditions the splitting of the D_2O signal amounted to 10.8 Hz. A total of 49 $^1D_{NH}$ and 39 $^1D_{C\alpha CO}$ dipolar couplings were used during the calculations. The axial component and rhombicity of the magnetic susceptibility tensor were determined by using histograms of the normalized residual dipolar couplings (*52*). Values of 11.3 Hz ($^1D_{NH}$) and 2.3 Hz ($^1D_{C\alpha CO}$) were obtained for the axial components and 0.08 for the rhombicity.

At all stages of the calculations, hydrogen-bond constraints were introduced for the residues showing typical NOE cross-peak patterns for α helices or β strands in the ^{15}N NOESY−HSQC and ^{13}C NOESY−HSQC spectra. For each hydrogen bond, two constraints were included into the calculations: $d_{NH\cdots O} = 1.8-2.4$ Å and $d_{N\cdots O} = 2.8-3.4$ Å.

Structures were visualized with the program MOLMOL (*53*).

Modeling of the [2Fe-2S] Cofactor and Its Environment. Because of the paramagnetism of the [2Fe-2S] cluster, signals from protons within a distance of about 7.8 Å from the iron ions are broadened out and are difficult to detect under standard NMR conditions (*54*). Different approaches have been applied in the past to circumvent the problem arising from the lack of meaningful NOEs in the proximity of the paramagnetic center, including the use of relaxation rates (*32, 55, 56*) and modeling based on structural homology (*30, 31, 33*). In this work, we primarily made use of the high degree of structural homology in this region among [2Fe-2S] ferredoxins, which allows for reliable modeling of the [2Fe-2S] cluster, but we also added two constraints based on relaxation rates.

During the DYANA calculations, constraints for modeling the [2Fe-2S] cluster, derived from X-ray data, were taken from the literature, following a previously described approach (*32*). In this case, a modified amino acid residue was introduced, comprising a cysteine moiety with an FeS group bound to S^{γ}. This new residue was implemented at positions 47 and 82, which define the two poles of the cluster. Additional distances used in the DYANA calculations to fix the cluster geometry are given in Table S1a (Supporting Information).

During the X-PLOR calculations, similar distance constraints were used for the [2Fe-2S] cofactor, which was introduced by binding one Fe_2S_2 group to residues 47 and 82 and adding all of the other information defining the cluster in the form of distance constraints (Table S1b, Supporting Information). The Fe−S distances of 2.29 Å implemented at this stage were recently determined by EXAFS studies of MMOR−Fd.[3]

In both cases, backbone dihedral angle constraints derived from the X-ray structure of the ferredoxin domain from PDR from *Pseudomonas cepacia* (PDB access code 2PIA) (*57*) were implemented in order to model residues Ser41-Cys50 and Leu80-Arg83, with allowed deviations of ±30°. This approach is based on the fact that the structure of the [2Fe-2S] cluster and its environment are highly conserved in all plant-type ferredoxins (*34*) and that this information has already been applied successfully in the determination of the solution structure of *Synechococcus elongatus* [2Fe-2S] ferredoxin (*33*). PDR, however, has backbone angles ψ_{Thr276}, ϕ_{Cys277}, ψ_{Cys277}, and ϕ_{Gly278} (corresponding to ψ_{Gly46}, ϕ_{Cys47}, ψ_{Cys47}, and ϕ_{Ala48} in MMOR−Fd) that differ significantly from those in similar [2Fe-2S] ferredoxins (Table S2, Supporting Information). The changes in the hydrogen-bonding network around the metal cluster arising from these differences bring about large differences in redox potentials, with the PDR value being −174 mV as compared to the −310 to −455 mV range encountered in most other

[3] Jackson, D. A., Merkx, M., Hedman, B., Lippard, S. J., and Hodgson, K. O. Unpublished results.

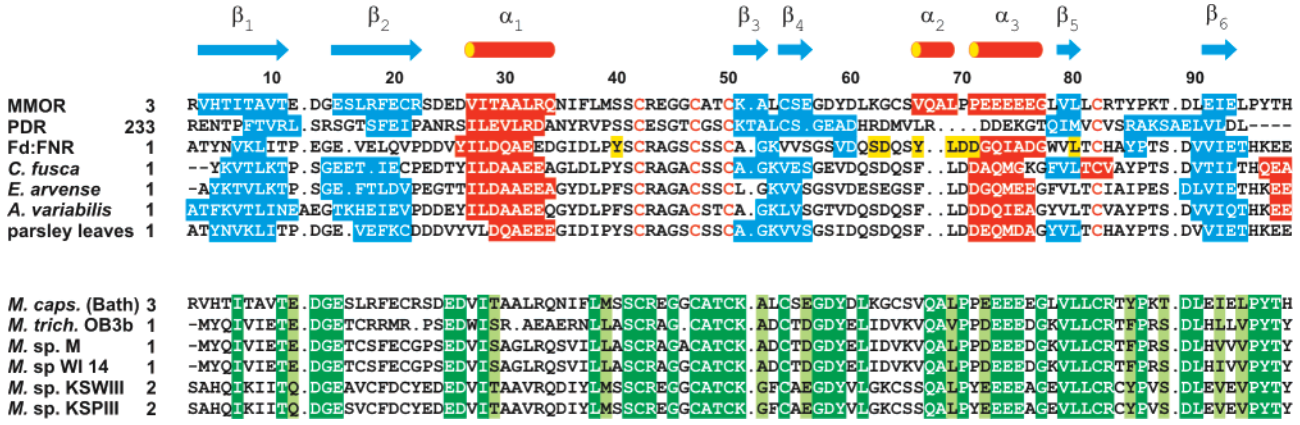

FIGURE 1: (Top) Sequence alignment and secondary structure of MMOR−Fd from *M. capsulatus* (Bath), PDR−Fd from *P. cepacia*, PDB code 2PIA (*57*), maize leaf ferredoxin from the Fd−FNR complex, 1GAQ (*68*), [2Fe-2S] ferredoxin from *Chlorella fusca*, 1AWD (*27*), [2Fe-2S] ferredoxin I from *Equisetum arvense*, 1FRR (*28*), [2Fe-2S] ferredoxin from *Anabaena variabilis* 7120, 1FXA (*69*), and [2Fe-2S] ferredoxin I from parsley leaves, 1PFD (*32*). Cysteine residues bound to the [2Fe-2S] cofactor are colored in red. Helices are denoted in red and β strands in blue. Secondary structures are as described in the respective PDB files. Residues labeled in yellow are on the contact surface between Fd and FNR. (Bottom) Sequence alignment of all known MMOR−Fd sequences from methanotrophic bacteria: *M. capsulatus* (Bath) (*70*, *71*), *Methylosinus trichosporium* OB3b (*72*, *73*), *Methylocystis* sp. strain M (*74*), *Methylocystis* sp. strain WI 14 (*75*), and *Methylomonas* sp. strains KSWIII and KSPIII (*76*). Identical and similar residues are denoted in dark and light green, respectively.

[2Fe-2S] ferredoxins (*58*−*60*). The ferredoxin redox potential in MMOR is −209 mV (*61*), which is close to that of PDR. After submitting our preliminary structure calculated without these additional dihedral angle constraints to the DALI server (*62*), we identified the ferredoxin domain in PDR to be structurally the second-most similar one to MMOR−Fd. A calculation using dihedral angles from the [2Fe-2S] protein determined to be the structurally most similar one, the ferredoxin from the green alga *Chlorella fusca* (*27*), resulted in higher values for the energy target function. This result supports the conclusion that the fold around the metal cluster found in PDR better describes the one in MMOR−Fd. The PDR structure was, therefore, used to model this part of the protein.

RESULTS

Backbone resonances of MMOR−Fd were assigned by using five triple-resonance experiments (HNCA, HN(CO)-CA, HN(CA)CB, HN(COCA)CB, and HNCO), ^{15}N selective labeling of leucine and valine, and reverse labeling of arginine residues as described previously (*39*, *63*). The secondary structure elements were identified by an analysis of short- and medium-range NOEs in the ^{15}N NOESY−HSQC and ^{13}C NOESY−HSQC spectra as well as by ^{13}C chemical shift indices (*64*). The protein consists of six β strands arranged in two sheets and three α helices. Figure 1 shows an overview of the secondary structure of MMOR−Fd.

A total of 1513 constraints were used for the structure calculation. These comprise 694 intraresidue, 198 sequential, 66 medium-range, and 166 long-range NOEs as well as 18 [2Fe-2S] cluster distance, 88 residual dipolar coupling, 217 dihedral angle, and 66 hydrogen-bond constraints (for 33 hydrogen bonds). Within the core region of the protein, residues 3−96, the family of 10 structures shown in Figure 2A has an average backbone rmsd of 0.55 Å with respect to the average structure. The structural statistics are summarized in Table 1. A ribbon diagram of MMOR−Fd is shown in Figure 2. Residues Val4-Thr11 and Glu15-Arg22 form strands β_1 and β_2, respectively. They are connected by a tight

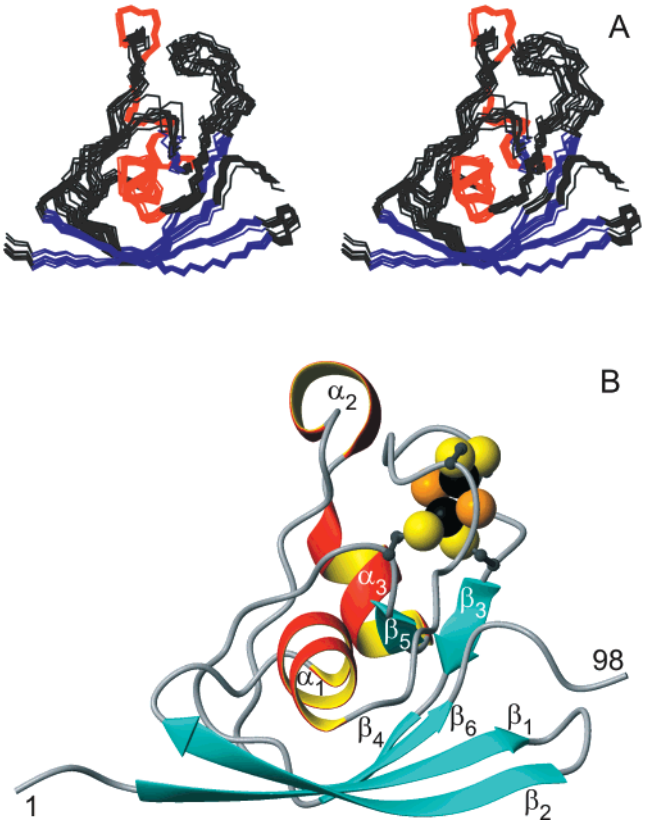

FIGURE 2: Solution structure of the reduced form of MMOR−Fd. (A) Stereoview of the backbone atoms (N, C$^\alpha$, and C) of 10 superimposed NMR-derived structures of MMOR−Fd (residues 3−96). β strands and α helices are shown in blue and red, respectively. The region close to the [2Fe-2S] cluster comprising residues Ser41-Cys50 and Leu80-Arg83 has been modeled by using dihedral angle constraints derived from the crystal structure of PDR (*57*), as described in the Materials and Methods section. (B) Ribbon diagram of MMOR−Fd in the same orientation.

turn to form a β hairpin, which is flanked by helix α_1 consisting of residues Val27-Gln34. This helix is followed by a long loop that contains three of the four cysteine residues coordinating to the [2Fe-2S] cluster (Cys42, Cys47, and Cys50). A short strand β_3 is formed from residues Lys51-

Table 1: Statistics for the MMOR−Fd Solution Structure

constraints	
NOE distance constraints	1124
intraresidue	694
sequential ($\|i-j\|=1$)	198
medium-range ($\|i-j\| \leq 4$)	66
$i, i+2$	31
$i, i+3$	21
$i, i+4$	14
long-range ($\|i-j\| \geq 5$)	166
H-bond constraints	66
[2Fe-2S] cluster constraints	18
dihedral angle constraints[a]	217
residual dipolar coupling constraints	88

average ensemble rmsd (Å) (residues 3−96)	
backbone	0.55
heavy atoms	1.03

[a] Dihedral angle constraints as obtained with TALOS (*43*) or generated using DYANA (*47*) based on NOE constraints.

Ala52, followed by another strand β_4 comprising residues Cys54-Glu56 which runs antiparallel to β_1. Two helices α_2 and glutamate-rich α_3 extend from residues Val66-Leu69 and Pro71-Gly77. They are connected by a tight turn containing a proline residue. Val79 and Leu80 form a short strand β_5 oriented antiparallel to β_3 and precede a loop containing the fourth cysteine (Cys82) coordinating to the iron−sulfur center. This loop is followed by strand β_6, which extends from residues Glu91-Glu93 and is located between β_1 and β_4 in the three-dimensional structure, running parallel to the first and antiparallel to the latter. All of the α helices are on the side of the protein containing the redox center, while all of the β strands constitute the distal surface.

In addition to the 31 hydrogen bonds that constitute the secondary structure elements, two other hydrogen bonds were identified. The first of these involves the side-chain amide nitrogen atom $N^{\epsilon 2}$ from residue Gln34 and the backbone carbonyl atom of Glu20 and packs α_1 behind β_1 and β_2 (Figure 3A). The existence of this hydrogen bond was deduced from the downfield-shifted resonance of the amide proton $H^{\epsilon 21}$ ($\delta = 9.05$ ppm) and the large number of cross-peaks in the ^{15}N NOESY−HSQC spectrum originating from this group (Figure 3B), suggesting a rigid conformation of the side chain. The other additional hydrogen bond had first only been postulated, on the basis of the sequence alignment of the reductase ferredoxin domain with other [2Fe-2S] proteins of known structure (Figure 1). In particular, the sequence alignment reveals the presence of a conserved serine residue (Ser65) located exactly 20 amino acids downstream from a universally conserved glycine residue (Gly45) within the iron−sulfur cluster for nearly all [2Fe-2S] proteins. A comparison of the respective structures shows a distinctive hydrogen bond from the backbone amide group of this serine to the backbone carbonyl atom of the glycine residue (Figure 4A). In the case of the ferredoxin domain from PDR, which does not contain a serine residue at this position, a methionine that is 19 amino acids away from the universally conserved glycine forms this hydrogen bond. Since MMOR also has a serine residue at this specific location, the existence of a hydrogen bond between Ser65 and Gly45 seemed likely. Because of the close proximity to the paramagnetic center, however, no cross-peaks could be observed in the NOESY spectra to check this assignment.

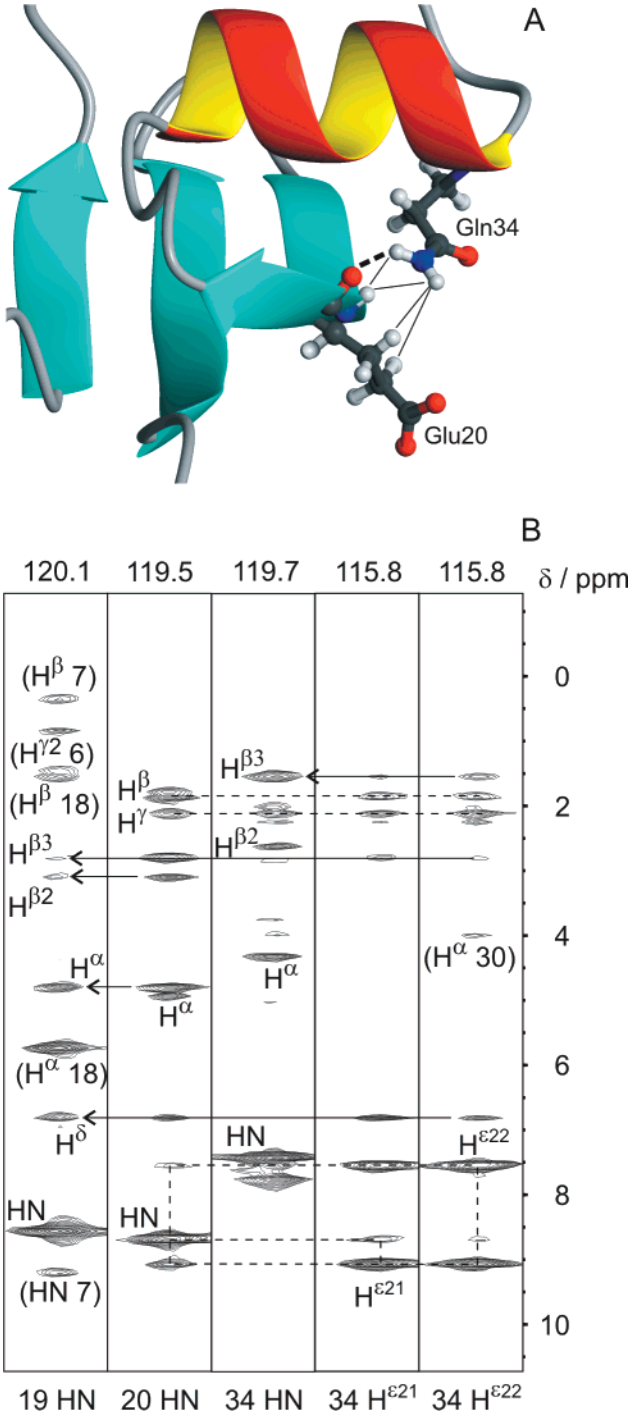

FIGURE 3: (A) Structure of MMOR−Fd showing a hydrogen bond from Gln34 $H^{\epsilon 21}$ to the backbone carbonyl group of Glu20 (- - -). (B) Selected strips from the ^{15}N NOESY−HSQC spectrum showing the unusually large number of cross-peaks for the side-chain amide group of Gln34, suggesting the involvement of $H^{\epsilon 21}$ in a hydrogen bond. The hydrogen-bond acceptor is identified as the backbone carbonyl group of Glu20 by cross-peaks to its amide and side-chain protons (- - -). These NOEs are shown in A as thin lines. Arrows indicate NOEs not explicitly shown in A.

A measurement of spin−lattice relaxation times $T_{1\rho}$ of the backbone amide nitrogen atoms led to an experimental confirmation of the proximity of Ser65 to the [2Fe-2S] cluster, supporting the existence of this putative hydrogen bond also in MMOR−Fd. As shown in Figure 4B, the relaxation times $T_{1\rho}$ are essentially the same over the whole protein, slightly larger than 90 ms, and become shorter only

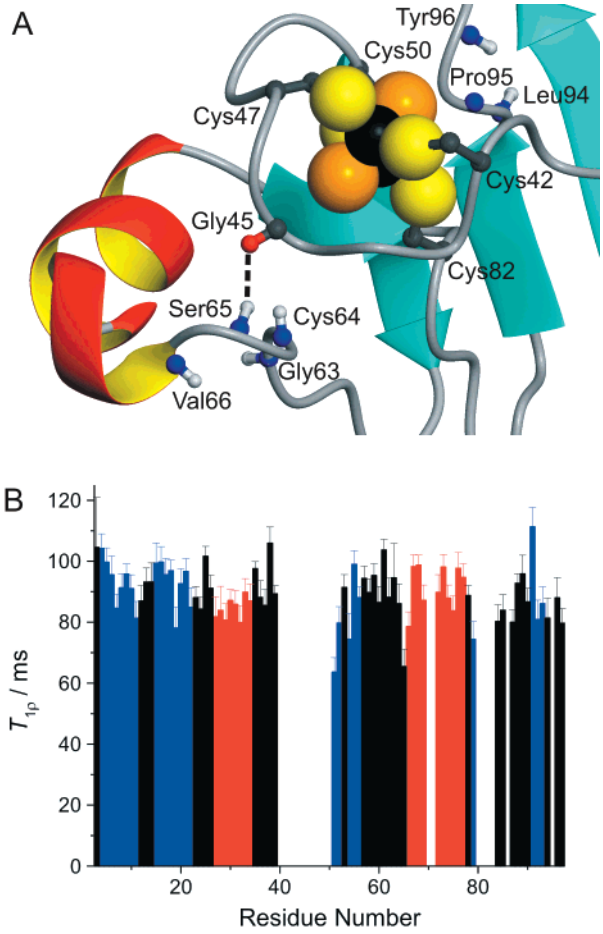

FIGURE 4: (A) Structure of MMOR−Fd showing a hydrogen bond in proximity to the [2Fe-2S] cluster (black, Fe; yellow, cysteine S; gold, inorganic S) pointing from the Ser65 NH to the backbone carbonyl group of Gly45. Several other backbone amide groups are also displayed. (B) Spin−lattice relaxation times $T_{1\rho}$ of the backbone amide nitrogen atoms. The secondary structural elements are color-coded (red, α helix; blue, β-strand). Residues not listed are either terminal, prolines, or in close proximity to the [2Fe-2S] cluster.

in the proximity of the paramagnetic center, being 64 ± 5 ms for Lys51 and 74 ± 6 ms for Val79, for example. Such a short $T_{1\rho}$ value also occurs for Ser65 (66 ± 7 ms), which indicates that this residue is similarly located in the vicinity of the [2Fe-2S] cluster, strongly supporting the occurrence of the postulated hydrogen bond.

Protein−Protein Binding Studies. The MMOH binding face of the MMOR ferredoxin domain was identified by means of an NMR titration experiment following a strategy previously described (*18, 45*). As explained in more detail in the Materials and Methods section, signals of bound MMOR−Fd are expected to be absent from the spectra owing to the high molecular weight of the MMOH/MMOR−Fd complex. Because of chemical exchange with the bound state, the lines of the free form should be broadened when excess MMOR−Fd is present. With increasing amounts of MMOH, such differential line broadening was indeed observed for the amide resonances in ^{15}N,^{1}H HSQC spectra of MMOR−Fd (Figure 5). Since an accurate determination of half-widths was technically difficult to achieve, the amount of line broadening was measured from the peak height maxima, which are inversely proportional to the line widths. This method also reduces possible integration errors that might be introduced in the case of slightly overlapping cross-peaks. The peak height Δ_i of each resonance i in the ^{15}N,^{1}H HSQC spectra of MMOR−Fd at different MMOH/MMOR−Fd ratios was determined according to eq 1, where $h_{0,i}$ and h_i are the peak height in free and complexed MMOR−Fd, as measured in the absence and presence of MMOH, respectively. The overbars indicate the average values of all of the resonances at the respective MMOH/MMOR−Fd ratio and were introduced for calibration purposes. Because of extreme line broadening of the resonances of free MMOR−Fd at a ratio of 1:2.4, only results for the first two experiments (1:10 and 1:6 ratios) were analyzed. The data obtained at both ratios yielded comparable results; we therefore discuss the results from the 1:10 experiment only.

$$\Delta_i = \frac{h_{0,i}}{\bar{h}_0} - \frac{h_i}{\bar{h}} \quad (1)$$

When the Δ values for the individual residues (Figure S1, Supporting Information) are mapped onto a surface plot of MMOR−Fd (parts A and C of Figure 6), it is evident that

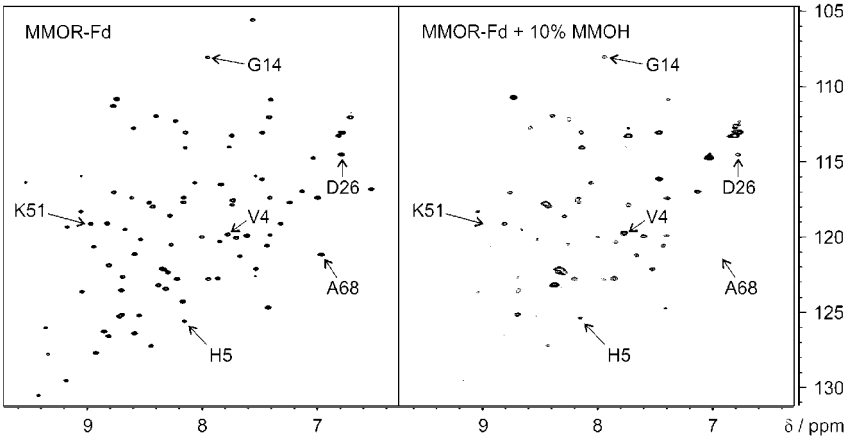

FIGURE 5: Differential line broadening in ^{15}N,^{1}H HSQC spectra of MMOR−Fd. Upon the addition of 10% MMOH, peaks corresponding to amide groups close to the binding surface display more than average line broadening (e.g., D26, Δ = 0.24; K51, Δ = 0.49; A68, Δ = 0.59), whereas peaks corresponding to amide groups away from the contact interface show less than average line broadening (e.g., V4, Δ = −0.84; H5, Δ = −0.36; G14, Δ = −0.27). Both spectra were recorded under otherwise identical conditions and are displayed at the same contour level.

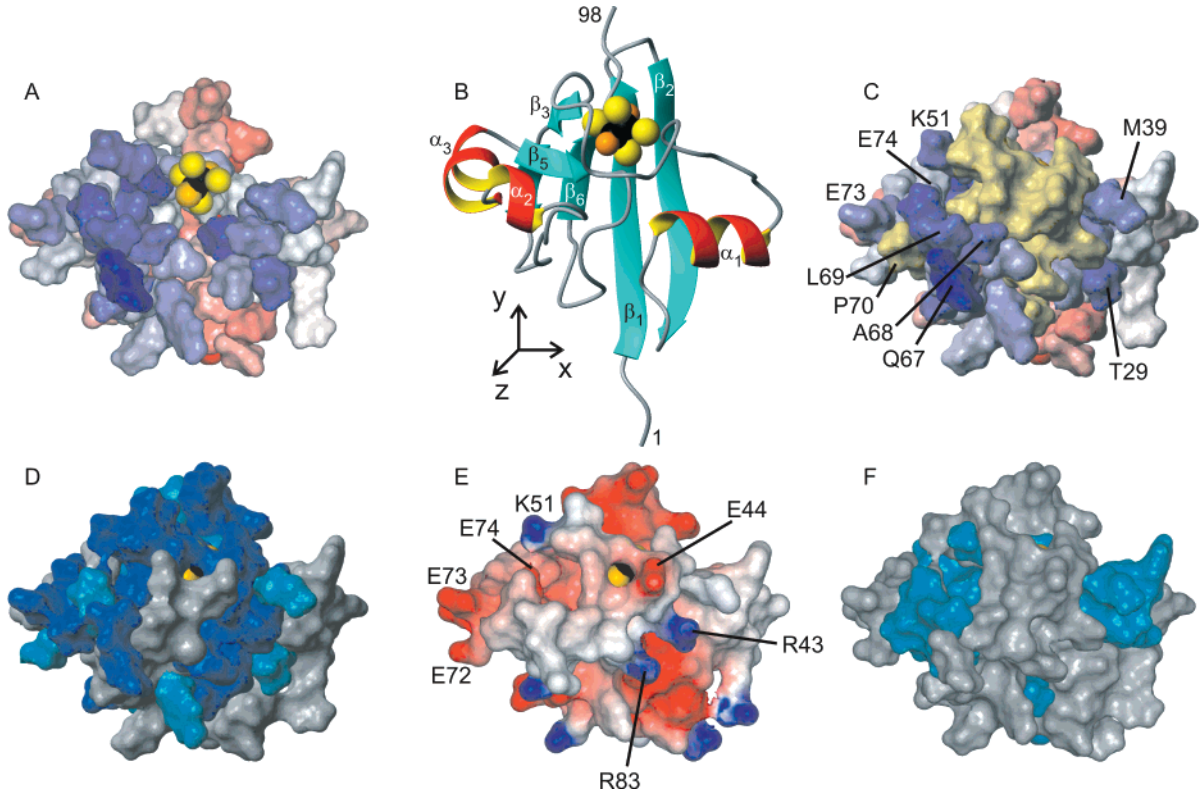

FIGURE 6: Mapping of binding data (A) onto a surface plot of the MMOR−Fd core (residues 4−94) shown in the same orientation as a ribbon diagram (B). The protein is rotated counterclockwise about 90° around first the *y*-axis and then the *x*-axis with respect to its orientation in Figure 2. In A, residues 40−50 and 80−83 are omitted to obtain a better view of the [2Fe-2S] cluster (black, Fe; yellow, cysteine S; gold, inorganic S) because these resonances are already broadened in the absence of MMOH. Because no binding data could be obtained for proline residues, they are also omitted. The binding data mapped in A are those obtained at a ratio of MMOH/MMOR−Fd of 1:10. Blue and red residues represent positive and negative values for Δ (eq 1) and, therefore, depict amino acids that are close and distant to the binding face, respectively. To obtain a more realistic view of the contact surface, binding (C), homology (D), electrostatic (E), and hydrophobicity (F) data are also mapped onto the complete surface of the protein core. In C, residues missing in A are marked in yellow. In D, identical and similar residues according to Figure 1 are marked in dark and light blue, respectively. In E, blue and red represent positive and negative partial charges, respectively. In F, all of the hydrophobic residues are shown in blue.

all of the amino acids with resonances that exhibit line broadening are located on the side of the protein that houses the [2Fe-2S] cluster and the α helices. Thus, this face appears to be the MMOH binding site. The residues least affected upon binding of the hydroxylase are located on the opposite side of the protein, which contains the *β* sheet. The location of the MMOH binding face identified in this way maps well onto the residues conserved among all of the MMOR proteins sequenced to date (Figure 6D). The electrostatic and hydrophobicity surface plots (parts E and F of Figure 6) suggest that the contact interface has a polar center with Arg43, Glu44, and Arg83 as charged residues and is surrounded by patches of hydrophobic residues.

DISCUSSION

The structure of the reduced $Fe^{II}Fe^{III}$ form of MMOR−Fd is similar to those of other plant-type [2Fe-2S] ferredoxins, despite their disparate physiological electron-transfer partners. Several key differences are apparent, however. One typical feature of the geometry of [2Fe-2S] proteins not covalently linked to their respective electron-transfer partners is a short α helix of amino acids with negatively charged side chains at the C terminus (*27*, *33*, *65*). In MMOR−Fd, this region neither displays a defined secondary structure nor contains residues with charged side chains. This difference is not entirely surprising, because in the full MMOR protein, the C terminus of the Fd domain links to the N terminus of the FAD domain. Furthermore, the lack of secondary structure at the C terminus might be indirectly correlated to the large difference in redox potentials between MMOR−Fd (−209 mV) (*61*) and most other [2Fe-2S] ferredoxins (−310 to −455 mV) (*58*−*60*). For PDR (*57*), which has a redox potential close to that of MMOR, theoretical calculations suggest that this difference is mainly due to changes in the hydrogen-bonding network around the metal cluster (*58*, *59*). This network is altered when a conserved serine, usually located between the second and third cysteine residues that bind to the iron atoms, is substituted by a glycine. In MMOR, it is substituted by alanine (Ala48), suggesting similarly altered hydrogen bonds. Because this serine usually serves as a hydrogen-bond donor with a conserved glutamate residue located in the C-terminal α helix as the acceptor (*26*), its substitution by an alanine renders the need for a hydrogen-bond acceptor at the C terminus unnecessary.

The aforementioned serine has been reported to play a central role in stabilizing the molecular surface of [2Fe-2S] proteins (*26*, *65*). Apparently, such stabilization is unnecessary in MMOR−Fd or is being achieved in a different way. It would be interesting to perform a systematic mutagenesis study with MMOR to investigate further and verify the above-mentioned conclusions. For example, would an A48S

mutation have a significant influence on the redox potential, even without the presence of negatively charged residues at the C terminus as possible hydrogen-bond acceptors?

A second feature that, to our knowledge, is unique among all [2Fe-2S] proteins is a helix−proline−helix motif involving helices α_2 and α_3. In this region, all MMOR proteins have a short, highly conserved sequence (QALP) that is not present in other plant-type [2Fe-2S] proteins. These residues are among the six amino acids most influenced upon the binding of MMOR−Fd to the hydroxylase protein (see the following discussion).

An interesting property of the MMOR−Fd sequence is the cluster of five consecutive glutamic acid residues from Glu72 to Glu76, which is partially conserved among MMOR proteins from other species. The solution structure presented here reveals that these residues are all part of helix α_3. Although other [2Fe-2S] ferredoxins from plants and algae are also α helical in this region, they do not reveal much sequence similarity with MMOR−Fd (Figure 1). Because approximately the first half of α_3, the conserved part of the Glu_5 sequence, is involved in binding the hydroxylase protein (see the following discussion), the accumulation of a large number of negatively charged residues at this location strongly suggests that they interact with a corresponding region of positively charged amino acids on MMOH.

The high sequence homology in MMOR proteins from different species suggests that the structures of the other five [2Fe-2S] domains fold in a manner very similar to that found here for MMOR−Fd and are likely to share the helix−proline−helix motif and the absence of secondary structure at the C terminus.

Binding Studies. The majority of residues experiencing line broadening upon the addition of MMOH are hydrophobic. Several residues for which no experimental data are available, owing to their close proximity to the paramagnetic diiron center, are polar, and most of them are uncharged. We, therefore, conclude that both hydrophobic and electrostatic packing forces are important for complex formation. This finding is consistent with results from other systems that utilize plant-type ferredoxins (*66*). The hydrophobic residues surrounding the ones housing the [2Fe-2S] cluster might serve as a template to minimize structural rearrangements at the dimetallic center during electron transfer. The participation of electrostatic forces in the binding interaction is consistent with the previous observation that MMOR and the regulatory protein MMOB do not compete for binding sites on the hydroxylase (*20*), because the interaction between MMOH and MMOB is mainly hydrophobic (*18*).

Because excess reductant was present during the titration experiments, we monitored MMOR−Fd binding to the reduced form of MMOH. The interaction surface most likely does not depend on the oxidation state, however. Binding studies of MMOB reveal essentially identical interactions with both reduced (*67*) and oxidized (*18*) MMOH.

The contact surface on MMOR−Fd is located in a region similar to that in the recently published complex between maize leaf [2Fe-2S] ferredoxin and Fd−$NADP^+$ oxidoreductase (*68*), a member of the flavoprotein electron transferase family with dissociable electron carriers. Several differences exist, however, one of them again involving the C-terminal region, which seems to be closer to the contact interface in the Fd−FNR complex. In contrast, several conserved residues of MMOR−Fd, located between Glu25 and Thr29, experience substantial line broadening during the titration of MMOR−Fd with MMOH that are not this close to the contact interface in the Fd−FNR complex. These subtle shifts in orientation of the contact surface are probably necessary in order to keep the [2Fe-2S] cluster within reach of both its electron-transfer partners, MMOH and the FAD moiety. Most of the residues at the contact interface of the Fd−FNR complex, labeled in yellow in Figure 1, are conserved in all of the [2Fe-2S] proteins except for MMOR−Fd and PDR−Fd and vice versa. This difference most likely reflects the need for specific recognition of the respective electron-transfer partner.

The titration data essentially confirm a previous prediction that residues Asp24-Gln34 form an α helix involved in complex formation with the hydroxylase. This postulate was based on an analysis of crystal packing of MMOH and inhibition studies with a synthetic peptide (*15*). As the MMOR−Fd solution structure shows, Val27-Gln34 do indeed form an α helix. Furthermore, the NMR-derived binding data indicate that the first half of this helix is close to the contact interface with MMOH, supporting the former conclusion based on crystal packing.

Three of the six residues with the largest amount of line broadening, Gln67, Ala68, and Leu69, are located in helix α_2, the first in the helix−proline−helix motif. This sequence is strictly conserved among MMOR proteins and has not yet been observed in other [2Fe-2S] ferredoxins. We, therefore, suggest that helix α_2 is absolutely necessary for binding to MMOH.

The good agreement between the NMR binding data and the positioning of conserved residues (Figure 6) leads to the conclusion that the full reductase protein binds the hydroxylase in the same manner as its individual ferredoxin domain. MMOR−Fd should, therefore, serve as a good model for MMOR in electron-transfer studies. For example, electron transfer between the [2Fe-2S] center in MMOR−Fd and the diiron center in the hydroxylase should occur without interference from the preceding intrareductase step. Such experiments are currently in progress.[2]

CONCLUSIONS

We have solved the structure of the reduced $Fe^{II}Fe^{III}$ form of the [2Fe-2S] domain of MMOR in solution, providing the first such information about the reductase component of any sMMO enzyme system. Its globular shape is similar to that of other [2Fe-2S] proteins, but its fold shows differences in the location of two α helices. A comparison of the putative MMOH binding site on MMOR−Fd with the contact surfaces of other ferredoxin proteins reveals that, although they are all located more or less in the same region of the protein, the different affinities for their distinct electron-transfer partners are achieved by having different conserved residues on the protein surface. The results presented here are an important contribution to our understanding of the mode of action of the MMO enzyme components, and they are a first step toward unraveling the structure of the complete methane monooxygenase reductase.

ACKNOWLEDGMENT

We thank Drs. P. Zhou and J. J. Chou for help in implementing residual dipolar coupling constraints, Dr. J. D. Gross for helpful discussions, and G. Heffron for technical assistance. Professor C. Luchinat provided valuable advice at the inception of this project, and Dr. M. Merkx provided the MMOH sample. J.M. is a Feodor Lynen fellow of the Alexander von Humboldt Foundation (Germany).

SUPPORTING INFORMATION AVAILABLE

Tables S1 and S2 and Figure S1 with distance constraints and a comparison of dihedral angles of different ferredoxin structures for selected residues in the [2Fe-2S] cluster and with binding data according to eq 1. This material is available free of charge via the Internet at http://pubs.acs.org.

REFERENCES

1. Ortiz de Montellano, P. R. (1995) *Cytochrome P450: Structure, Mechanism, and Biochemistry*, 2nd ed., Plenum Press, New York.
2. Small, F. J., and Ensign, S. A. (1997) *J. Biol. Chem. 272*, 24913−24920.
3. Pessione, E., Divari, S., Griva, E., Cavaletto, M., Rossi, G. L., Gilardi, G., and Giunta, C. (1999) *Eur. J. Biochem. 265*, 549−555.
4. Pikus, J. D., Studts, J. M., Achim, C., Kauffmann, K. E., Münck, E., Steffan, R. J., McClay, K., and Fox, B. G. (1996) *Biochemistry 35*, 9106−9119.
5. Newman, L. M., and Wackett, L. P. (1995) *Biochemistry 34*, 14066−14076.
6. Merkx, M., Kopp, D. A., Sazinsky, M. H., Blazyk, J. L., Müller, J., and Lippard, S. J. (2001) *Angew. Chem., Int. Ed. 40*, 2782−2807.
7. Que, L., Jr., and Dong, Y. (1996) *Acc. Chem. Res. 29*, 190−196.
8. Liu, K. E., and Lippard, S. J. (1995) *Adv. Inorg. Chem. 42*, 263−289.
9. Wallar, B. J., and Lipscomb, J. D. (1996) *Chem. Rev. 96*, 2625−2657.
10. Higgins, I. J., Best, D. J., Hammond, R. C., and Scott, D. (1981) *Microbiol. Rev. 45*, 556−590.
11. Colby, J., and Dalton, H. (1978) *Biochem. J. 171*, 461−468.
12. Colby, J., Stirling, D. I., and Dalton, H. (1977) *Biochem. J. 165*, 395−402.
13. Whittington, D. A., Sazinsky, M. H., and Lippard, S. J. (2001) *J. Am. Chem. Soc. 123*, 1794−1795.
14. Whittington, D. A., Rosenzweig, A. C., Frederick, C. A., and Lippard, S. J. (2001) *Biochemistry 40*, 3476−3482.
15. Rosenzweig, A. C., Brandstetter, H., Whittington, D. A., Nordlund, P., Lippard, S. J., and Frederick, C. A. (1997) *Proteins 29*, 141−152.
16. Rosenzweig, A. C., Frederick, C. A., Lippard, S. J., and Nordlund, P. (1993) *Nature 366*, 537−543.
17. Elango, N., Radhakrishnan, R., Froland, W. A., Wallar, B. J., Earhart, C. A., Lipscomb, J. D., and Ohlendorf, D. H. (1997) *Protein Sci. 6*, 556−568.
18. Walters, K. J., Gassner, G. T., Lippard, S. J., and Wagner, G. (1999) *Proc. Natl. Acad. Sci. U.S.A. 96*, 7877−7882.
19. Chang, S.-L., Wallar, B. J., Lipscomb, J. D., and Mayo, K. H. (1999) *Biochemistry 38*, 5799−5812.
20. Gassner, G. T., and Lippard, S. J. (1999) *Biochemistry 38*, 12768−12785.
21. Fox, B. G., Froland, W. A., Dege, J. E., and Lipscomb, J. D. (1989) *J. Biol. Chem. 264*, 10023−10033.
22. Lund, J., and Dalton, H. (1985) *Eur. J. Biochem. 147*, 291−296.
23. Lund, J., Woodland, M. P., and Dalton, H. (1985) *Eur. J. Biochem. 147*, 297−305.
24. Colby, J., and Dalton, H. (1979) *Biochem. J. 177*, 903−908.
25. Fox, B. G., Hendrich, M. P., Surerus, K. K., Andersson, K. K., Froland, W. A., Lipscomb, J. D., and Münck, E. (1993) *J. Am. Chem. Soc. 115*, 3688−3701.
26. Morales, R., Charon, M.-H., Hudry-Clergeon, G., Pétillot, Y., Norager, S., Medina, M., and Frey, M. (1999) *Biochemistry 38*, 15764−15773.
27. Bes, M. T., Parisini, E., Inda, L. A., Saraiva, L. M., Peleato, M. L., and Sheldrick, G. M. (1999) *Structure 7*, 1201−1211.
28. Ikemizu, S., Bando, M., Sato, T., Morimoto, Y., Tsukihara, T., and Fukuyama, K. (1994) *Acta Crystallogr., Sect. D 50*, 167−174.
29. Berman, H. M., Westbrook, J., Feng, Z., Gilliland, G., Bhat, T. N., Weissig, H., Shindyalov, I. N., and Bourne, P. E. (2000) *Nucleic Acids Res. 28*, 235−242.
30. Mo, H., Pochapsky, S. S., and Pochapsky, T. C. (1999) *Biochemistry 38*, 5666−5675.
31. Pochapsky, T. C., Jain, N. U., Kuti, M., Lyons, T. A., and Heymont, J. (1999) *Biochemistry 38*, 4681−4690.
32. Im, Y.-C., Liu, G., Luchinat, C., Sykes, A. G., and Bertini, I. (1998) *Eur. J. Biochem. 258*, 465−477.
33. Baumann, B., Sticht, H., Schärpf, M., Sutter, M., Haehnel, W., and Rösch, P. (1996) *Biochemistry 35*, 12831−12841.
34. Lelong, C., Sétif, P., Bottin, H., André, F., and Neumann, J.-M. (1995) *Biochemistry 34*, 14462−14473.
35. Pochapsky, T. C., Ye, X. M., Ratnaswamy, G., and Lyons, T. A. (1994) *Biochemistry 33*, 6424−6432.
36. Weber, N., and Strotmann, H. (1993) *Biochim. Biophys. Acta 1143*, 204−210.
37. Matsubara, H., and Saeki, K. (1992) *Adv. Inorg. Chem. 38*, 223−280.
38. Neri, D., Szyperski, T., Otting, G., Senn, H., and Wüthrich, K. (1989) *Biochemistry 28*, 7510−7516.
39. Ferentz, A. E., and Wagner, G. (2000) *Q. Rev. Biophys. 33*, 29−65.
40. Peng, J. W., and Wagner, G. (1994) in *Nuclear Magnetic Resonance Probes of Molecular Dynamics* (Tycko, R., Ed.), pp 373−454, Kluwer Academic Publishers, Dordrecht, The Netherlands.
41. Peng, J. W., Thanabal, V., and Wagner, G. (1991) *J. Magn. Reson. 94*, 82−100.
42. Bartels, C., Xia, T.-H., Billeter, M., Güntert, P., and Wüthrich, K. (1995) *J. Biomol. NMR 5*, 1−10.
43. Cornilescu, G., Delaglio, F., and Bax, A. (1999) *J. Biomol. NMR 13*, 289−302.
44. Wagner, G. (1997) *Nat. Struct. Biol. 4*, 841−844.
45. Matsuo, H., Walters, K. J., Teruya, K., Tanaka, T., Gassner, G. T., Lippard, S. J., Kyogoku, Y., and Wagner, G. (1999) *J. Am. Chem. Soc. 121*, 9903−9904.
46. Güntert, P., Braun, W., and Wüthrich, K. (1991) *J. Mol. Biol. 217*, 517−530.
47. Güntert, P., Mumenthaler, C., and Wüthrich, K. (1997) *J. Mol. Biol. 273*, 283−298.
48. Brünger, A. T. (1992) X-PLOR, Version 3.1: A System for X-ray Crystallography and NMR, Yale University Press, New Haven, CT.
49. Mori, S., Abeygunawardana, C., O'Neil Johnson, M., and van Zijl, P. C. M. (1995) *J. Magn. Reson., Ser. B 108*, 94−98.
50. Yang, D., Venters, R. A., Mueller, G. A., Choy, W. Y., and Kay, L. E. (1999) *J. Biomol. NMR 14*, 333−343.
51. Hansen, M. R., Mueller, L., and Pardi, A. (1998) *Nat. Struct. Biol. 5*, 1065−1074.
52. Clore, G. M., Gronenborn, A. M., and Bax, A. (1998) *J. Magn. Reson. 133*, 216−221.
53. Koradi, R., Billeter, M., and Wüthrich, K. (1996) *J. Mol. Graphics 14*, 51−55.
54. Oh, B.-H., and Markley, J. L. (1990) *Biochemistry 29*, 3993−4004.
55. Bertini, I., Donaire, A., Luchinat, C., and Rosato, A. (1997) *Proteins 29*, 348−358.
56. Bertini, I., and Luchinat, C. (1996) *Coord. Chem. Rev. 150*, 1−296.

57. Correll, C. C., Batie, C. J., Ballou, D. P., and Ludwig, M. L. (1992) *Science 258*, 1604−1610.
58. Li, J., Nelson, M. R., Peng, C. Y., Bashford, D., and Noodleman, L. (1998) *J. Phys. Chem. A 102*, 6311−6324.
59. Correll, C. C., Ludwig, M. L., Bruns, C. M., and Karplus, P. A. (1993) *Protein Sci. 2*, 2112−2133.
60. Cammack, R., Rao, K. K., Bargeron, C. P., Hutson, K. G., Andrew, P. W., and Rogers, L. J. (1977) *Biochem. J. 168*, 205−209.
61. Kopp, D. A., Gassner, G. T., Blazyk, J. L., and Lippard, S. J. (2001) *Biochemistry*, in press.
62. Holm, L., and Sander, C. (1993) *J. Mol. Biol. 233*, 123−138.
63. Chou, J. J., Matsuo, H., Duan, H., and Wagner, G. (1998) *Cell 94*, 171−180.
64. Wishart, D. S., and Sykes, B. D. (1994) *J. Biomol. NMR 4*, 171−180.
65. Hurley, J. K., Weber-Main, A. M., Stankovich, M. T., Benning, M. M., Thoden, J. B., Vanhooke, J. L., Holden, H. M., Chae, Y. K., Xia, B., Cheng, H., Markley, J. L., Martínez-Júlvez, M., Gómez-Moreno, C., Schmeits, J. L., and Tollin, G. (1997) *Biochemistry 36*, 11100−11117.
66. Walker, M. C., Pueyo, J. J., Navarro, J. A., Gómez-Moreno, C., and Tollin, G. (1991) *Arch. Biochem. Biophys. 287*, 351−358.
67. Chang, S.-L., Wallar, B. J., Lipscomb, J. D., and Mayo, K. H. (2001) *Biochemistry 40*, 9539−9551.
68. Kurisu, G., Kusunoki, M., Katoh, E., Yamazaki, T., Teshima, K., Onda, Y., Kimata-Ariga, Y., and Hase, T. (2001) *Nat. Struct. Biol. 8*, 117−121.
69. Rypniewski, W. R., Breiter, D. R., Benning, M. M., Wesenberg, G., Oh, B.-H., Markley, J. L., Rayment, I., and Holden, H. M. (1991) *Biochemistry 30*, 4126−4131.
70. Coufal, D. E., Blazyk, J. L., Whittington, D. A., Wu, W. W., Rosenzweig, A. C., and Lippard, S. J. (2000) *Eur. J. Biochem. 267*, 2174−2185.
71. Stainthorpe, A. C., Lees, V., Salmond, G. P. C., Dalton, H., and Murrell, J. C. (1990) *Gene 91*, 27−34.
72. Fox, B. G., Liu, Y., Dege, J. E., and Lipscomb, J. D. (1991) *J. Biol. Chem. 266*, 540−550.
73. Cardy, D. L. N., Laidler, V., Salmond, G. P. C., and Murrell, J. C. (1991) *Arch. Microbiol. 156*, 477−483.
74. McDonald, I. R., Uchiyama, H., Kambe, S., Yagi, O., and Murrell, J. C. (1997) *Appl. Environ. Microbiol. 63*, 1898−1904.
75. Grosse, S., Laramee, L., Wendlandt, K.-D., McDonald, I. R., Miguez, C. B., and Kleber, H.-P. (1999) *Appl. Environ. Microbiol. 65*, 3929−3935.
76. Shigematsu, T., Hanada, S., Eguchi, M., Kamagata, Y., Kanagawa, T., and Kurane, R. (1999) *Appl. Environ. Microbiol. 65*, 5198−5206.

BI015668K